PHYSICAL REVIEW B **95**, 241403(R) (2017)

Suppression of exciton-exciton annihilation in tungsten disulfide monolayers encapsulated by hexagonal boron nitrides

Yusuke Hoshi,[1,*] Takashi Kuroda,[2] Mitsuhiro Okada,[3] Rai Moriya,[1] Satoru Masubuchi,[1] Kenji Watanabe,[2] Takashi Taniguchi,[2] Ryo Kitaura,[3] and Tomoki Machida[1,†]

[1]*Institute of Industrial Science, University of Tokyo, 4-6-1 Komaba, Meguro-ku, Tokyo 153-8505, Japan*

[2]*National Institute for Materials Science, 1-1 Namiki, Tsukuba, Ibaraki 305-0044, Japan*

[3]*Department of Chemistry, Nagoya University, Furocho, Chikusa-ku, Nagoya 464-8603, Japan*

(Received 13 March 2017; revised manuscript received 15 May 2017; published 7 June 2017)

We investigates exciton-exciton annihilation (EEA) in tungsten disulfide (WS_2) monolayers encapsulated by hexagonal boron nitride (hBN). It is revealed that decay signals observed by time-resolved photoluminescence (PL) are not strongly dependent on the exciton densities of hBN-encapsulated WS_2 monolayers (WS_2/hBN). In contrast, the sample without the bottom hBN layer (WS_2/SiO_2) exhibits a drastic decrease of decay time with increasing exciton density due to the appearance of a rapid PL decay component, signifying nonradiative EEA-mediated recombination. Furthermore, the EEA rate constant of WS_2/hBN was determined as $(6.3 \pm 1.7) \times 10^{-3}$ cm^2 s^{-1}, being about 2 orders of magnitude smaller than that of WS_2/SiO_2. Thus, the observed EEA rate reduction played a key role in enhancing luminescence intensity at high exciton densities in the WS_2 monolayer.

DOI: 10.1103/PhysRevB.95.241403

Two-dimensional transition-metal dichalcogenides (TMDs) offer a unique platform for realizing an ideal, atomically thin, and optically accessible two-dimensional system. In particular, TMDs of MX_2 stoichiometry (M = Mo, W; X = S,Se,Te) are considered promising materials for fundamental physics research, exhibiting unique properties such as direct bandgaps of single monolayers (1L) and extraordinary large binding energies [1–4]. These properties lead to exciton formation even at room temperature, with their recombination dynamics being important for TMD applications in optoelectronic devices [5–11]. The optical properties of 1L-TMDs are quite sensitive to the nature of supporting substrates [12] and other environmental conditions [13,14], which induce changes of background doping levels and the exciton recombination rate.

The enhanced many-body effects arising from strong interactions between excitons at high exciton density are another prominent feature of low-dimensional systems. Among the numerous processes of multiexciton dynamics, involving species such as charged excitons, [15,16], biexcitons [17,18], and exciton-trion complexes [19], exciton-exciton annihilation (EEA) is one of the most extensively studied ones [20–29]. EEA is a scattering mechanism in which two excitons come into contact, with one of them undergoing nonradiative recombination and transferring its energy to another exciton that is then excited to a high-energy continuum state. Subsequently, the excited exciton undergoes thermal relaxation without emitting light. This process is identical to the Auger relaxation of inner-shell electrons following the photoionization of atoms, being a source of luminescence quenching. EEA occurs at ultrafast time scales of several picoseconds, limiting the radiative decay of excitons under intense photoexcitation. Thus, EEA suppression is critical for enhancing the performance of optoelectronic devices. The recently reported EEA rate constants of suspended TMDs are of the order of $\sim 10^{-1}$ cm^2 s^{-1}, giving rise to EEA at a markedly small exciton density of $\sim 10^{10}$ cm^{-2} [24,26]. In contrast, the corresponding rate constants of TMDs supported by SiO_2 films are smaller [23,25,26], still being about two orders of magnitude larger than those of conventional two-dimensional quantum wells such as ZnCdSe/ZnSe heterostructure [30]. Interactions of excitons with their surroundings may suppress nonradiative EEA-mediated recombination in TMDs. Hexagonal boron nitride (hBN) is a prominent atomically flat dielectric surrounding material for layered structures such as graphene and TMDs, reducing their surface roughness and charged impurity scattering of carriers [31,32]. Thus, encapsulation of layered materials by hBN is advantageous not only for device-related applications, but also for investigating the fundamental physics of these materials. TMDs encapsulated by hBN have been reported to exhibit significantly narrow spectral lines with reduced inhomogeneous broadening [33]. In this study, we focus on the behavior of excitons in the EEA process occurring in 1L-WS_2 encapsulated by hBN (hBN/WS_2), with WS_2 chosen as a model material due to its low defect density and a high PL yield at room temperature as compared to those of other TMDs [25,26,34,35]. Furthermore, molecular adsorption and/or photoinduced quenching was avoided by forming an hBN layer on top of the 1L-WS_2. We demonstrate that encapsulation of 1L-WS_2 by hBN helps to achieve an EEA rate constant of $(6.3 \pm 1.7) \times 10^{-3}$ cm^2 s^{-1}, which is about two orders of magnitude smaller than that of hBN/WS_2 directly deposited on SiO_2 films.

1L-WS_2 was grown using the following process sequence: Deposition of a 10–30-nm-thick W layer on a sapphire substrate by sputtering, thermal oxidation at 700 °C, and sulfurization at 900 °C [36]. Bulk hBN crystals were grown by employing a temperature-gradient method at high pressure (4.0–5.5 GPa) and high temperature (1500−1750 °C) [37]. Flakes of hBN were prepared by micromechanical exfoliation of bulk crystals. Two heterostructured samples were fabricated on a 300-nm-thick SiO_2 on n^+-doped Si (100) using the stamping technique through a dry peel/lift process. The first sample comprised 1L-WS_2 encapsulated by hBN, with the

*Corresponding author: yuhoshi@iis.u-tokyo.ac.jp
†tmachida@iis.u-tokyo.ac.jp

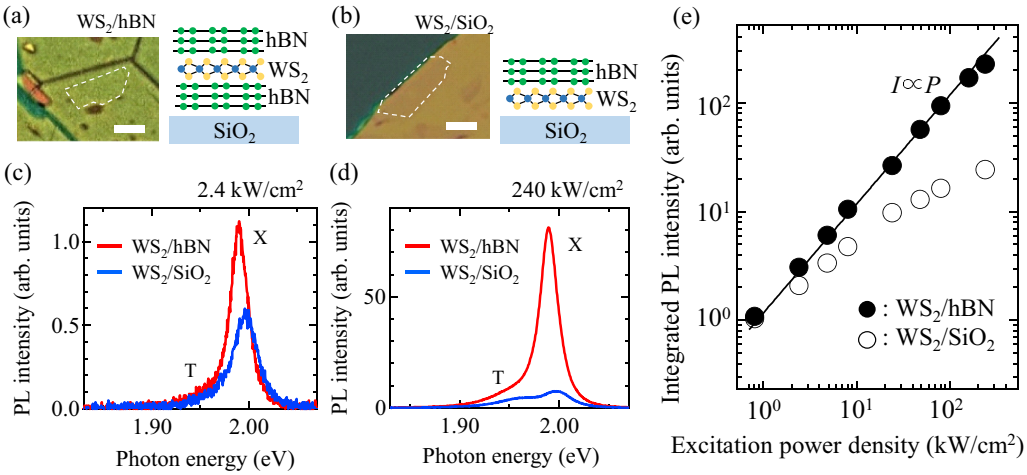

FIG. 1. Optical microscopy images and schematic structures of (a) WS_2/hBN and (b) WS_2/SiO_2 heterostructured samples. White broken lines in (a) depict 1L-WS_2 regions. The scale bar is 5 μm long. Steady-state PL spectra of WS_2/hBN (red) and WS_2/SiO_2 (blue) at an excitation power of (c) 2.4 kW cm^{-2} and (d) 240 kW cm^{-2}. All spectral line shapes were fitted using a combination of Gaussian and Lorentzian functions. (e) Integrated spectral intensities of the X peak plotted as a function of excitation power for WS_2/hBN (filled circles) and WS_2/SiO_2 (open circles). The solid line represents a linear fit of the data obtained for WS_2/hBN.

top-to-bottom layer sequence being hBN/1L-WS_2/hBN/SiO_2 [Fig. 1(a)]. The second sample, serving as a reference, comprised hBN/1L-WS_2 directly formed on SiO_2 without the bottom hBN layer [Fig. 1(b)]. These two samples are further denoted as WS_2/hBN (hBN-encapsulated) and WS_2/SiO_2 (SiO_2-supported).

A standard confocal microscope with a focusing diameter of $\sim$1 μm was used to observe the luminescence of 1L-WS_2. Steady-state photoluminescence (PL) measurements were carried out using a continuous wave excitation laser emitting at 532 nm and a spectrometer equipped with a cooled charge-coupled device detector. Time-resolved PL (TRPL) measurements were carried out using an optical parametric oscillator generating picosecond pulses with a wavelength of 550 nm and a repetition rate of 76 MHz. PL decay curves were analyzed by a synchronously scanned streak camera with a minimum temporal resolution of 2 ps. All measurements were performed at room temperature and ambient pressure.

Figures 1(a) and 1(b) show optical microscopy images of WS_2/hBN and WS_2/SiO_2 samples, respectively, and Fig. 1(c) shows the steady-state PL spectra of each sample at low excitation power (2.4 kW cm^{-2}). The above samples exhibit similar spectra, featuring an intense peak at $\sim$1.99 eV and a small side peak at 1.95 eV, attributed to neutral excitons (X) and negative trions (T), respectively. The FWHM of the exciton peak of WS_2/hBN and WS_2/SiO_2 is 21 and 29 meV, respectively. These values are comparable to that of 1L-WS_2 directly grown on an hBN template [38], indicating that no crystal damage is inflicted during heterostructure fabrication. Figure 1(e) shows the dependence of exciton peak intensity on excitation power, revealing that WS_2/SiO_2 exhibits a sublinear dependence in the entire power range, with intensity saturation occurring at excitation powers around 100 kW cm^{-2}. This behavior is typical of power-induced nonradiative recombination, as confirmed for other TMD systems [23,28,39,40]. In contrast, the intensities exhibited by WS_2/hBN are strictly proportional to excitation power up to $\sim$100 kW cm^{-2}, which marks the onset of saturation. The observed luminescence robustness with respect to input power is specific to the hBN-encapsulated sample. Consequently, at sufficiently high excitation power (e.g., 240 kW cm^{-2}), the PL

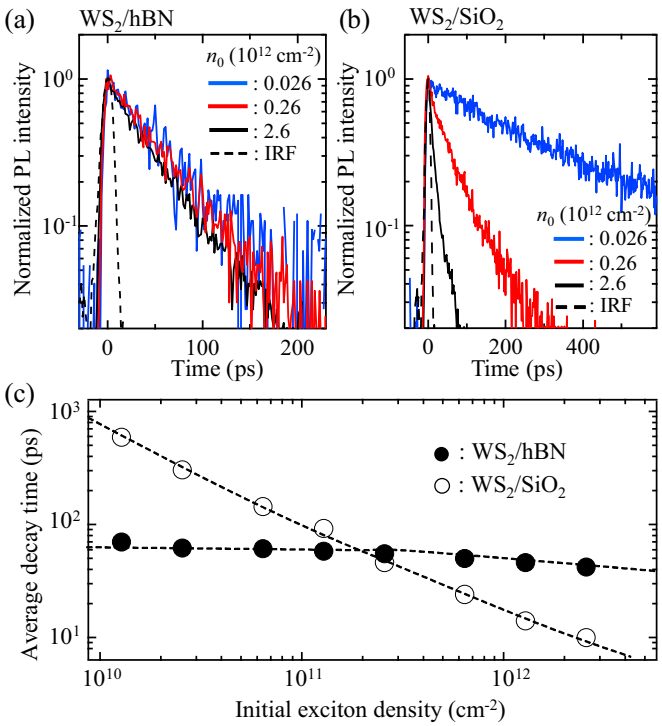

FIG. 2. Normalized exciton PL decay signals for (a) WS_2/hBN and (b) WS_2/SiO_2 at different initial exciton densities. Instrumental response function (IRF) signals are shown for reference as dashed lines. (c) Average decay times as functions of initial exciton densities for WS_2/hBN (filled circles) and WS_2/SiO_2 (open circles). Broken lines serve as viewing guides. Average decay times were determined as the inverse of intensity-weighted decay rates, which were calculated by phenomenological double-exponent fitting of the measured decay signal.

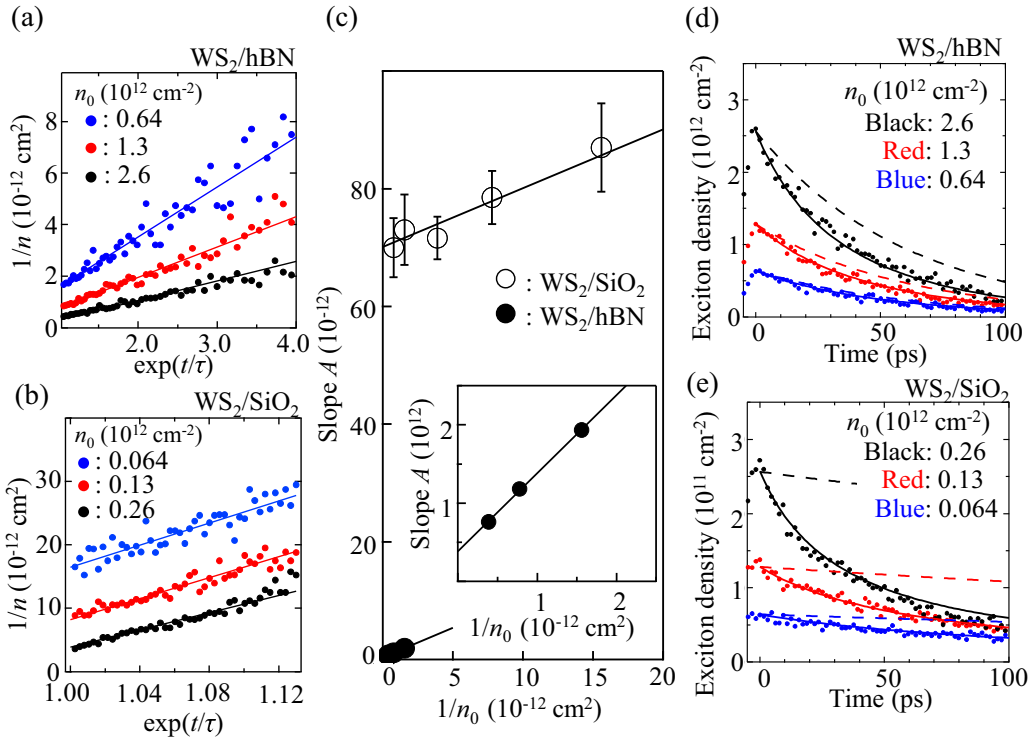

FIG. 3. Data expressed in the linearized form of Eq. (2) for (a) WS_2/hBN and (b) WS_2/SiO_2 heterostructures, with n_0 denoting the initial exciton density and lines representing linear fits to the above data. (c) The slope $(1/n_0 + \gamma\tau)$ of linear fits as a function of reciprocal initial exciton density for WS_2/hBN (filled circles) and WS_2/SiO_2 (open circles). Inset shows the zoomed-in region for WS_2/hBN. Decay curves derived from Eq. (2) at various initial exciton densities for (d) WS_2/hBN and (e) WS_2/SiO_2. Filled circles represent experimental results, solid lines denote decay curves reproduced by Eq. (2), and dashed lines represent monoexponential decay curves ($n = n_0 \times \exp(t/\tau)$).

intensity of WS_2/hBN is an order of magnitude higher than that of WS_2/SiO_2 [Fig. 1(d)].

To demonstrate that encapsulation by hBN strongly affects exciton dynamics in 1L-WS_2, we systematically investigated neutral exciton decay time by TRPL measurements. Figure 2(a) shows PL decay signals of WS_2/hBN normalized with respect to initial exciton densities. Density estimation was performed by calculating the photon flux per pulse, and 1L-WS_2 was assumed to exhibit a linear absorbance of 3.5% for simplicity, independent of the substrate choice [41]. Decay signals observed at initial exciton densities below $2.6 \times 10^{11}\,\mathrm{cm}^{-2}$ are almost the same, being well described by a monoexponential curve with a time constant τ_{hBN} of ~60 ps. At a high exciton density of $2.6 \times 10^{12}\,\mathrm{cm}^{-2}$, the data can no longer be fitted by a monoexponential curve due to the appearance of a rapid decay component in the first 50 ps, which is more clearly seen in Fig. 3(d), where the experimental data is plotted in a linear scale axis without the normalization. Figure 2(b) shows the exciton PL decay signals of WS_2/SiO_2, with that for the lowest exciton density ($2.6 \times 10^{10}\,\mathrm{cm}^{-2}$) described by a monoexponential curve with a decay time τ_{SiO_2} of 590 ps. Significantly faster decay is observed for a tenfold-higher exciton density ($2.6 \times 10^{11}\,\mathrm{cm}^{-2}$), with the average decay time decreasing to 46 ps. Herein, we utilized the average decay time as an alternative to the decay time, since the measured signal deviated from monoexponential decay behavior. The average decay time is defined as the inverse of intensity-weighted decay rates, which are calculated by double-exponent fitting of the experimental curve. A further increase of exciton density to $2.6 \times 10^{12}\,\mathrm{cm}^{-2}$ resulted in a steeper decay with an average decay time constant of 10 ps. (See Supplemental Material [42] for the IRF signal and the exciton PL decay signal for a WS_2/SiO_2.) Notably, the transient intensity at 0 ps is roughly proportional to initial exciton density. (See Supplemental Material [42] for the result of PL decay signals at various initial exciton densities.) Thus, the measured exciton density-dependent decay time is purely governed by the probability of nonradiative recombination. Figure 2(c) shows a summary of extracted decay times for two samples as functions of initial exciton densities. For WS_2/SiO_2, decay times steeply decrease with exciton density, remaining unchanged for WS_2/hBN under the same conditions (except for a small reduction at high exciton densities). As previously reported [22,23,25–27], the decreased dependence of decay time on initial exciton density is thought to be caused by EEA-mediated nonradiative recombination.

To quantitatively evaluate EEA rate constants for WS_2/hBN and WS_2/SiO_2, we focus on exciton PL decay signals at high initial exciton densities, where the EEA-mediated optical transition occurs. The decay of exciton density n accounting for the EEA term is described by

$$\frac{dn}{dt} = -\frac{n}{\tau} - \gamma n^2, \tag{1}$$

where γ is the EEA rate constant, and τ is the excitonic decay time in the absence of EEA [25,27,43]. For a time-independent

TABLE I. EEA rate constant of the WS_2/hBN and WS_2/SiO_2 samples given in this study.

	WS_2/hBN	WS_2/SiO_2
EEA rate constant ($cm^2\,s^{-1}$)	$(6.3 \pm 1.7) \times 10^{-3}$	$(1.2 \pm 0.1) \times 10^{-1}$

annihilation rate constant γ, the linear solution of Eq. (1) can be represented by

$$\frac{1}{n} = Ae^{t/\tau} - \gamma\tau, \tag{2}$$

where A equals $(1/n_0 + \gamma\tau)$, and n_0 is the initial exciton density. The intensity-dependent data for WS_2/hBN and WS_2/SiO_2 are replotted in the linear form given by Eq. (2) [Figs. 3(a) and 3(b)], with A determined as the slope of the corresponding linear fit including the error. Figure 3(c) shows a plot of A as a function of $1/n_0$ for both samples. The above results are successfully fitted by a linear function with a tilt of 1. EEA rate constants γ are estimated from the values of A at $1/n_0 = 0$. The estimated EEA rate constants are given in Table I. Notably, the γ value of WS_2/hBN ($(6.3 \pm 1.7) \times 10^{-3}\,cm^2\,s^{-1}$) is much smaller than that of WS_2/SiO_2 ($(1.2 \pm 0.1) \times 10^{-1}\,cm^2\,s^{-1}$) which, in turn, is very similar to the rate constant ($\sim 10^{-1}\,cm^2\,s^{-1}$) of 1L-$WS_2$ directly deposited on SiO_2 [25,26]. The error bars of the rate constant are brought in the linear fitting for inducing the slope A. To verify the validity of the obtained EEA rate constants, they are used to reproduce the decay curves using Eq. (2), achieving good agreement with experimental results for both WS_2/hBN and WS_2/SiO_2 [Figs. 3(d) and 3(e), respectively]. In contrast, the decay curves calculated from the above rate equation without the EEA term ($n = n_0 \times \exp(t/\tau)$) obviously deviate from the experimental results for both samples. Thus, the reduction of decay time dependence on initial exciton density is caused by the EEA-mediated optical transition, with the rate constant of WS_2/hBN being about two orders of magnitude smaller than that of WS_2/SiO_2. This result strongly indicates that encapsulation by hBN allows the EEA-mediated nonradiative recombination in 1L-WS_2 to be suppressed.

In general, the EEA rate constant is known to be proportional to the exciton diffusion constant D and the separation R of two excitons at the point of EEA occurrence [26,43]. At first, we discuss the effect of D on the EEA rate constant of WS_2/hBN. Considering the mechanisms of carrier mobility enhancement in graphene encapsulated by hBN [44], the value of D for WS_2/hBN should exceed that of WS_2/SiO_2. Thus, the exciton diffusion coefficient is not related to the extraordinarily small EEA rate constant of WS_2/hBN. On the other hand, encapsulation by hBN decreases the exciton binding energy because of the change in the dielectric environment [14,45]. The encapsulation could subsequently increase R since the exciton Bohr radius increases with decreasing exciton binding energy [46], accelerating the EEA. Thus, the separation R of two excitons cannot also explain the extraordinarily small EEA rate constant of WS_2/hBN. To rationalize the abovementioned EEA rate constant, we proposed a model based on uniform exciton dispersion in the 2D plane. For 1L-WS_2 on SiO_2, excitons may be localized due to potential fluctuation in 1L-WS_2 owing to the roughness of the 1L-WS_2/SiO_2 interface and the fixed charges in the vicinity of the SiO_2 surface [47]. In this case, the localized exciton density should be larger than the injected exciton density due to exciton collection in the potential minima of 1L-WS_2. Therefore, EEA-mediated nonradiative recombination in WS_2/SiO_2 probably occurs at a lower injected exciton density. On the other hand, encapsulation by hBN enables the generation of delocalized excitons in 1L-WS_2 due to the smaller interface roughness and the separation from charged impurities in SiO_2. In fact, the faster PL signal decay observed at low exciton densities [Fig. 2(c)] suggests the existence of delocalized excitons in WS_2/hBN. When uniformly dispersed in the 2D plane, these excitons are easily captured at crystal defects, explaining the quick PL signal decay of low-density delocalized excitons [48]. Additionally, we measured steady-state PL spectra of these samples under cryogenic conditions (around 4 K) and found that strong bound exciton emissions are clearly observed only for the WS_2/SiO_2 sample (not shown). For WS_2/hBN, exciton delocalization should contribute to the extraordinarily small rate constant of EEA, which occurs upon contact of two excitons.

As a guide for further luminescence yield enhancement at high exciton densities, we calculated the time-integrated form $\int n(t)dt$ of exciton density derived from Eq. (2) (see Supplemental Material [42] for the dependence of the time-integrated exciton density on the annihilation rate constant), which should correspond to the luminescence intensity generated by 1L-WS_2. For samples with large EEA rate constants, the exciton PL decay time does not strongly affect the time integration of exciton density. In contrast, for samples with smaller EEA rate constants, such as WS_2/hBN, an increase in PL decay time can enhance luminescence intensity. The exciton PL decay time τ is related to the radiative decay time τ_r and the nonradiative decay time τ_{nr} of excitons: $1/\tau = 1/\tau_r + 1/\tau_{nr}$, with τ_r predicted to be of the order of several nanoseconds [49]. Therefore, reducing the number of nonradiative recombination centers such as S vacancies should drastically enhance the luminescence intensity of samples with smaller EEA rate constants. For example, the quantum yield of 1L-WS_2 has recently been reported to reach a value close to unity after treatment with a nonoxidizing organic superacid [50]. Thus, larger luminescence yields might be realized by suppressing nonradiative pathways involving crystal defects in hBN-encapsulated 1L-WS_2.

In conclusion, we systematically investigated the effect of encapsulation by hBN on the exciton transition through the EEA in the 1L-WS_2, which takes place at high exciton density. It was found that the luminescence robustness with respect to input power was specific to the hBN-encapsulated sample. We quantitatively evaluated the EEA rate constant of the hBN-encapsulated 1L-WS_2 by using time-resolved PL measurements and demonstrated that the EEA rate constant of the WS_2/hBN was about two orders of magnitude smaller than that of WS_2/SiO_2, indicating that the hBN encapsulation results in high quantum yields at high exciton density in 1L-WS_2. Earlier experiments on 1L-MoS_2[33] suggested the encapsulation by hBN layers made it possible to access its intrinsic high optical quality owing to the surface protection and substrate flatness. Also, for 1L-WS_2 in the present study, the hBN encapsulation revealed the extraordinarily small

EEA rate constant. Thus, the encapsulation by hBN could be a rational design for wide variety of TMD materials in optoelectronics and fundamental physics.

This work was partly supported by the Japan Science and Technology Agency (JST), the Core Research for Evolutional Science and Technology (CREST) through Grant No. JPMJCR15F3; JSPS KAKENHI through Grants No. JP25107003, No. JP25107004, No. JP15K21722, No. JP26248061, No. JP25107002, and No. JP16H00982; and by a Sasagawa Scientific Research Grant from The Japan Science Society.

[1] K. F. Mak, K. He, C. Lee, G. H. Lee, J. Hone, T. F. Heinz, and J. Shan, Nat. Mater. **12**, 207 (2013).
[2] A. Chernikov, T. C. Berkelbach, H. M. Hill, A. Rigosi, Y. Li, O. B. Aslan, D. R. Reichman, M. S. Hybertsen, and T. F. Heinz, Phys. Rev. Lett. **113**, 076802 (2014).
[3] K. He, N. Kumar, L. Zhao, Z. Wang, K. F. Mak, H. Zhao, and J. Shan, Phys. Rev. Lett. **113**, 026803 (2014).
[4] H. M. Hill, A. F. Rigosi, C. Roquelet, A. Chernikov, T. C. Berkelbach, D. R. Reichman, M. S. Hybertsen, L. E. Brus, and T. F. Heinz, Nano Lett. **15**, 2992 (2015).
[5] J. S. Ross, P. Klement, A. M. Jones, N. J. Ghimire, J. Yan, D. G. Mandrus, T. Taniguchi, K. Watanabe, K. Kitamura, W. Yao, D. H. Cobden, and X. Xu, Nat. Nanotechnol. **9**, 268 (2014).
[6] F. Withers, O. D. Pozo-Zamudio, A. Mishchenko, A. P. Rooney, A. Gholinia, K. Watanabe, T. Taniguchi, S. J. Haigh, A. K. Geim, A. I. Tartakovskii, and K. S. Novoselov, Nat. Mater. **14**, 301 (2015).
[7] D. Li, R. Cheng, H. Zhou, C. Wang, A. Yin, Y. Chen, N. O. Weiss, Y. Huang, and X. Duan, Nat. Commun. **6**. 7509 (2015).
[8] F. Withers, O. D. Pozo-Zamudio, S. Schwarz, S. Dufferwiel, P. M. Walker, T. Godde, A. P. Rooney, A. Gholinia, C. R. Woods, P. Blake, S. J. Haigh, K. Watanabe, T. Taniguchi, I. L. Aleiner, A. K. Geim, V. I. Fal'ko, A. I. Tartakovskii, and K. S. Novoselov, Nano Lett. **15**, 8223 (2015).
[9] A. Pospischil, M. M. Furchi, and M. Mueller, Nat. Nanotechnol. **9**, 257 (2014).
[10] M. Bernardi, M. Palummo, and J. C. Grossman, Nano Lett. **13**, 3664 (2013).
[11] B. W. H. Baugher, H. O. H. Churchill, Y. Yang, and P. Jarillo-Herrero, Nat. Nanotechnol. **9**, 262 (2014).
[12] M. Buscema, G. A. Steele, H. S. J. van der Zant, and A. Castellanos-Gomez, Nano Res. **7**, 561 (2014).
[13] S. Tongay, J. Zhou, C. Ataca, J. Liu, J. S. Kang, T. S. Matthews, L. You, J. Li, J. C. Grossman, and J. Wu, Nano Lett. **13**, 2831 (2013).
[14] Y. Lin, X. Ling, L. Yu, S. Huang, A. L. Hsu, Y.-H. Lee, J. Kong, M. S. Dresselhaus, and T. Palacios, Nano Lett. **14**, 5569 (2014).
[15] K. Kheng, R. T. Cox, Y. Merle d'Aubigné, F. Bassani, K. Saminadayar, and S. Tatarenko, Phys. Rev. Lett. **71**, 1752 (1993).
[16] G. Finkelstein, H. Shtrikman, and I. Bar-Joseph, Phys. Rev. B **53**, R1709 (1996).
[17] Q. Fu, D. Lee, A. Mysyrowicz, A. V. Nurmikko, R. L. Gunshor, and L. A. Kolodziejski, Phys. Rev. B **37**, 8791 (1988).
[18] R. Cingolani, Y. Chen, and K. Ploog, Phys. Rev. B **38**, 13478 (1988).
[19] A. Singh, G. Moody, S. Wu, Y. Wu, N. J. Ghimire, J. Yan, D. G. Mandrus, X. Xu, and X. Li, Phys. Rev. Lett. **112**, 216804 (2014).
[20] A. Suna, Phys. Rev. B **1**, 1716 (1970).
[21] L. Lüer, S. Hoseinkhani, D. Polli, J. Crochet, T. Hertel, and G. Lanzani, Nat. Phys. **5**, 54 (2009).
[22] N. Kumar, Q. Cui, F. Ceballos, D. He, Y. Wang, and H. Zhao, Phys. Rev. B **89**, 125427 (2014).
[23] S. Mouri, Y. Miyauchi, M. Toh, W. Zhao, G. Eda, and K. Matsuda, Phys. Rev. B **90**, 155449 (2014).
[24] S. Konabe and S. Okada, Phys. Rev. B **90**, 155304 (2014).
[25] L. Yuan and L. Huang, Nanoscale **7**, 7402 (2015).
[26] Y. Yu, Y. Yu, C. Xu, A. Barrette, K. Gundogdu, and L. Cao, Phys. Rev. B **93**, 201111 (2016).
[27] A. Surrente, A. A. Mitioglu, K. Galkowski, L. Klopotowski, W. Tabis, B. Vignolle, D. K. Maude, and P. Plochocka, Phys. Rev. B **94**, 075425 (2016).
[28] C. Robert, R. Picard, D. Lagarde, G. Wang, J. P. Echeverry, F. Cadiz, P. Renucci, A. Högele, T. Amand, X. Marie, I. C. Gerber, and B. Urbaszek, Phys. Rev. B **94**, 155425 (2016).
[29] G. Froehlicher, E. Lorchat, and S. Berciaud, Phys. Rev. B **94**, 085429 (2016).
[30] R. A. Taylor, R. A. Adams, J. F. Ryan, and R. M. Park, J. Cryst. Growth **159**, 822 (1996).
[31] X. Cui, G.-H. Lee, Y. D. Kim, G. Arefe, P. Y. Huang, C.-H. Lee, D. A. Chenet, X. Zhang, L. Wang, F. Ye, F. Pizzocchero, B. S. Jessen, K. Watanabe, T. Taniguchi, D. A. Muller, T. Low, P. Kim, and J. Hone, Nat. Nanotechnol. **10**, 534 (2015).
[32] S. Behura, P. Nguyen, S. Che, R. Debbarma, and V. Berry, J. Am. Chem. Soc. **137**, 13060 (2015).
[33] F. Cadiz, E. Courtade, C. Robert, G. Wang, Y. Shen, H. Cai, T. Taniguchi, K. Watanabe, H. Carrere, D. Lagarde, M. Manca, T. Amand, P. Renucci, S. Tongay, X. Marie, and B. Urbaszek, Phys. Rev. X **7**, 021026 (2017).
[34] N. Peimyoo, J. Shang, C. Cong, X. Shen, X. Wu, E. K. L. Yeow, and T. Yu, ACS Nano **7**, 10985 (2013).
[35] X.-X. Zhang, Y. You, S. Y. F. Zhao, and T. F. Heinz, Phys. Rev. Lett. **115**, 257403 (2015).
[36] H. R. Gutiérrez, N. Perea-López, A. L. Elías, A. Berkdemir, B. Wang, R. Lv, F. López-Urías, V. H. Crespi, H. Terrones, and M. Terrones, Nano Lett. **13**, 3447 (2013).
[37] K. Watanabe, T. Taniguchi, and H. Kanda, Nat. Mater. **3**, 404 (2004).
[38] M. Okada, T. Sawazaki, K. Watanabe, T. Taniguchi, H. Hibino, H. Shinohara, and R. Kitaura, ACS Nano **8**, 8273 (2014).
[39] J. Shang, X. Shen, C. Cong, N. Peimyoo, B. Cao, M. Eginligil, and T. Yu, ACS Nano **9**, 647 (2015).
[40] S. Mouri, Y. Miyauchi, and K. Matsuda, Nano Lett. **13**, 5944 (2013).
[41] Y. Li, A. Chernikov, X. Zhang, A. Rigosi, H. M. Hill, A. M. van der Zande, D. A. Chenet, E.-M. Shih, J. Hone, and T. F. Heinz, Phys. Rev. B **90**, 205422 (2014).
[42] See Supplemental Material at http://link.aps.org/supplemental/10.1103/PhysRevB.95.241403 for the IRF signal and the exciton PL decay signal, PL decay signals at various initial exciton densities, and the time-integrated exciton density plotted as a function of the EEA rate constant.

[43] P. E. Shaw, A. Ruseckas, and I. D. W. Samuel, Adv. Mater. **20**, 3516 (2008).

[44] C. R. Dean, A. F. Young, I. Meric, C. Lee, L. Wang, S. Sorgenfrei, K. Watanabe, T. Taniguchi, P. Kim, K. L. Shepard, and J. Hone, Nat. Nanotechnol. **5**, 722 (2010).

[45] A. V. Stier, N. P. Wilson, G. Clark, X. Xu, and S. A. Crooker, Nano Lett. **16**, 7054 (2016).

[46] G. Bastard, E. E. Mendez, L. L. Chang, and L. Esaki, Phys. Rev. B **26**, 1974 (1982).

[47] P. J. Caplan, E. H. Poindexter, B. E. Deal, and R. R. Razouk, J. Appl. Phys. **50**, 5847 (1979).

[48] H. Hillmer, A. Forchel, R. Sauer, and C. W. Tu, Phys. Rev. B **42**, 3220 (1990).

[49] M. Palummo, M. Bernardi, and J. C. Grossman, Nano Lett. **15**, 2794 (2015).

[50] M. Amani, P. Taheri, R. Addou, G. H. Ahn, D. Kiriya, D.-H. Lien, J. W. Ager III, R. M. Wallace, and A. Javey, Nano Lett. **16**, 2786 (2016).